Kinetic Analysis on Non-isothermal Combustion of Several Urban Biomass Fuels

Ying Wang, Qing-hai Pang,* Zhi-jun He,* Ji-hui Liu, Jun-hong Zhang, and Wen-long Zhan

Thermogravimetric combustion characteristics of ginkgo leaves (GK), pine needles (PN), corn straw (CS), aspen leaves (AS), and white poplar leaves (WP) were studied. Results showed that the combustion of selected samples consisted of at least two weight loss stages. Besides, characteristic temperatures lagged towards high temperature zones under high heating rate, which was considered as the effect of insufficient transfer of heat. The combustion of volatile compounds and char from PN and CS was isolated under high heating rate and consequently the exothermic rate around 300 °C was intensified and the exothermic rate over 400 °C was decreased, while the maximum heat release rates of GK, AS, and WP were transferred into high temperature zones with the increasing of heating rate. The average activation energy of PN and CS was high though their combustion completed at a lower temperature, which was possibly due to the low average energy of molecules in samples in low temperature environment. The aromaticity, degree of condensation, CH_2/CH_3, and structure parameters of oxygen-containing functional groups were calculated according to the peak areas derived from the convolution of FTIR spectra. These parameters explained the discrepancy in both reactivity and exothermic behaviors of biomass samples during combustion.

Keywords: Thermogravimetric analysis; Biomass; Kinetics of combustion; Heating rate

Contact information: Research Institute of Mass Energy Optimization and New Technology of Metallurgy, University of Science and Technology Liaoning, Anshan, Liaoning, China;
** Corresponding authors: hzhj2002@126.com; edikitty@126.com*

INTRODUCTION

The increasing industrial depletion of fossil fuels and deterioration of the human resident environment in China has been attracting attention due to the enormous Chinese industrial capacity (Hoel 1996). Annually, a huge amount of coal and petroleum are being consumed at an industrial scale, and consequently a large quantity of particulate matter and greenhouse gases are being generated. As a result, many major cities have been frequently suffering from the phenomenon of fog and haze, which is considered to be closely related to the particulate matter produced by the wide application of coal-based and petrolic fossil fuels during industrial production and manufacture (Zhang *et al*. 2015). In order to maintain the contribution of industrial development on the Chinese economy, policies have been issued to mediate the contradiction between industrial expansion and human ecological environment. Therefore, it becomes urgent for Chinese researchers to explore new energy sources to realize the "green development" of Chinese industry.

Biomass energy is a widely distributed, carbon neutral, environmentally friendly energy source, and hence it has received increasing attention from all over the world (Caputo *et al*. 2005; Zeng *et al*. 2007; Abbasi and Abbasi 2010; Qin *et al*. 2017). China, as an agricultural country with vast yield and territory, generates a huge amount of by-products from agricultural production and green plants. Although the chronic oxidation and spontaneous combustion of these biomasses will both increase the emission of CO_2 and the possibility of conflagration in wild areas, these by-products are still not well collected and utilized in China at present. On the contrary, if above biomasses can be well collected and classified as an energy source for industrial application, not only the discharge of greenhouse gases will be partly decreased but also the possibility for natural disasters will be reduced. Thus, the development of by-products from agriculture and plants as a sustainable energy resource is conducive to reduce the dependence of industry on fossil fuels (Zhou and Wu 2005; Ying and Jiang 2007).

Many studies have evaluated the application possibility of biomass in different industrial links. Combustion behavior of agricultural residues such as miscanthus, poplar wood, and rice husk was studied by Mustafa *et al*. (2013) with thermogravimetric analysis. The results indicated that the reactivity of biomass can be attributed to the formation of volatile compounds, while the energy releases from biomass fuels during combustion is related to the proportion of fixed carbon. Emre *et al*. (2012) analyzed the co-combustion behavior of biomass fuels and oil shale blends and found that the addition of biomass lowers the ignition temperature and facilitates the combustion property of oil shale in blends. The addition of biomass will increase the proportion of volatile in blends and stabilize the ignition and combustion of blends; consequently, a superior combustion of blends is achieved with 10% or 20% addition of biomass into oil shale. Mustafa *et al*. (2017) investigated the combustion characteristics of main components of lignocellulose, cellulose, hemicellulose and lignin in biomass (hazelnut shell) and noticed that the average activation energy of these compounds in biomass varies between 83.8 and 191.7 $kJ \cdot mol^{-1}$ for both OFW and KAS methods. Kandasamy *et al*. (2017) studied the combustion of poplar wood, hazelnut shell, and wheat bran and revealed that the reactivity of biomass is related to the content of light volatile, while the quantity of heat releases during the combustion is determined by the content of fixed carbon in biomass.

The overall aim of this research was to investigate the combustion behavior of by-products from common urban plants and acquire the reaction mechanism of various components at different stages of combustion, which is critical for the further application of these biomass fuels in industrial or civil scale. Hence, non-isothermal thermogravimetric combustion experiments on by-products from five common urban plants under low heating rates were conducted in this research in order to separate the independent combustion peaks from conversion rate curves and kinetic studies were also carried out with Flynn-Wall-Ozawa (FWO) method. As a result, the combustion sequence of components in biomass samples was determined, while the activation energy values of samples at different conversion rates were also calculated. Meanwhile, Fourier transform infrared spectroscopy (FTIR) was also introduced to analyze the functional group structures of selected samples and explain the difference in reactivity of these biomasses during combustion. Eventually, the feasibility and reaction condition of various biomasses for industrial application can be analyzed based on above results.

EXPERMENTAL

Materials and Preparation

Biomass samples of ginkgo leaves (GK), pine needles (PN), corn straw (CS), aspen leaves (AS), and white poplar leaves (WP) were collected in autumn from urban areas of Anshan city, which is located in the northeastern part of China. The original morphology of selected biomass samples are shown in Fig. 1. All biomass samples were dried at a temperature of 100 ± 5 °C for 8 h, then crushed and sieved to a particle sized below 0.074mm.

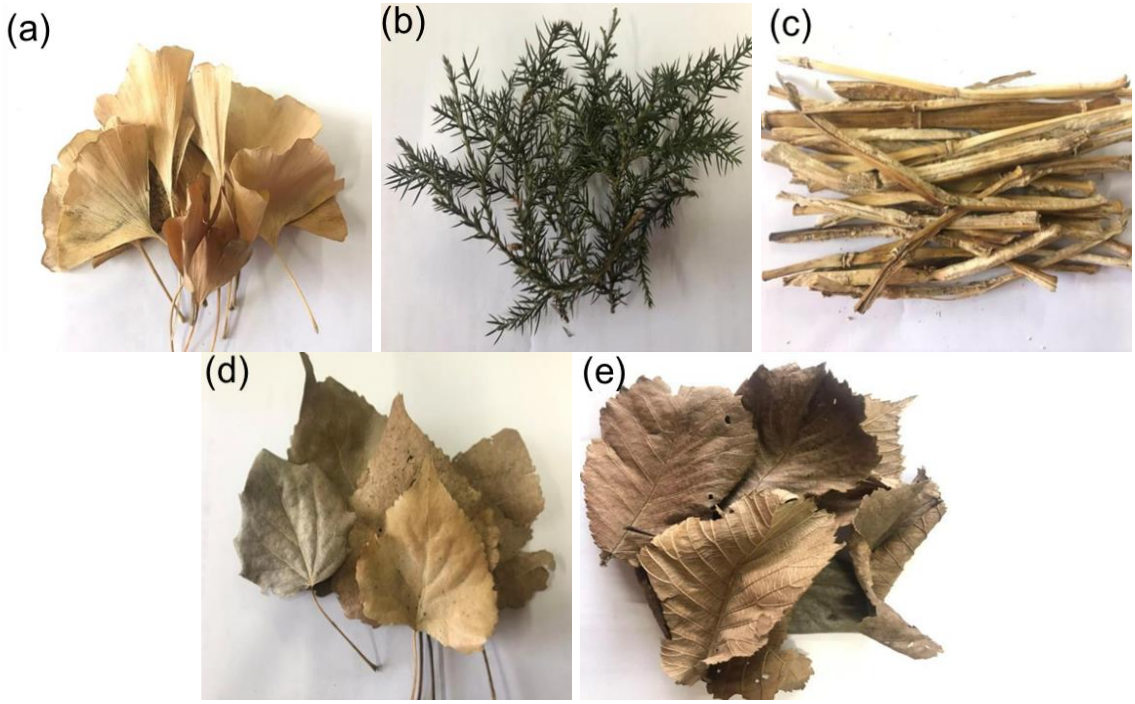

Fig. 1. Original morphology of biomass samples: (a) GK; (b) PN; (c) CS; (d) AS; and (e) WP

The proximate and ultimate analyses of biomass samples were conducted respectively according to the requirements of GB/T 30732-2014 and the results are listed in Table 1. Though the fixed carbon in PN and CS are higher compared to other biomass, the oxygen content in PN and CS is also observed to be higher. Consequently, the heat released during the combustion of PN and CS is relatively lower than other biomasses.

Table 1. Proximate and Ultimate Analysis of Samples

Sample	Proximate Analysis (wt. %)			Ultimate Analysis (wt. %)					HHV (MJ/kg)
	FC_d	V_d	A_d	C_d	H_d	O_d	N_d	S_d	
GK	17.84	71.33	10.83	45.02	4.69	37.42	1.85	0.21	15.24
PN	18.15	75.92	5.93	50.80	7.01	35.89	3.10	0.25	20.82
CS	21.44	76.42	2.14	42.71	4.87	35.29	1.12	0.28	15.11
AS	13.70	67.22	19.08	59.35	9.76	30.35	2.17	0.97	28.68
WP	12.71	70.73	16.56	59.41	8.41	32.78	1.95	1.48	26.31

Notes: A, ash; V, volatile matter; FC, fixed carbon; d, dry basis; HHV, high calorific value.

Methods

Thermogravimetric (TG) characteristics of biomass samples were determined by using a HCT-4 thermogravimetric analyzer (Henven Scientific Instrument Factory, Beijing, China) in air atmosphere. Approximately 5 mg sample was loaded into a corundum crucible (Φ 3 mm × 4.5 mm) and then heated to 600 °C at various heating rates (5, 10 and 20 °C/min).

A small quantity of sample was applied to reduce the temperature gradient between surface and center of sample, while a flow rate of 100 mL/min was also testified to be sufficient for the venting of gas products and supporting of sample combustion. In order to eliminate the influence of gas flow and buoyancy generated by thermal expansion, tests without sample were done to collect the baseline data for thermogravimetric experiments. Besides, each experiment was conducted at least three times to ensure an ideal reproducibility of all experiments.

The fraction conversion (α) of biomass sample during combustion can be derived with Eq. 1,

$$\alpha = \frac{W_0 - W_t}{W_0 - W_\infty} \quad (1)$$

where W_0 represents the initial mass of sample, W_t represents the sample mass at t time and W_∞ represents the residual mass of the sample after reaction.

RESULTS AND DISCUSSION

Thermogravimetric Analysis

The conversion rate and reaction rate curves of all biomass samples are shown in Fig. 2. All reaction rate curves consisted of at least two independent stages during the combustion process.

Weight loss in the first stage ranged from 200 to 400 °C and was identified to be pyrolysis of cellulose and hemicellulose, while the second stage above 400 °C was classified as the decomposition of lignin and combustion of char generated in the first stage (Liu *et al*. 2018). Moreover, the maximum reaction rate of samples increased with the increasing of heating rate, while the corresponding temperature of maximum reaction rate was also observed to be moving towards higher temperature zones.

The variation just described can be explained based on the fact that samples were able to be heated to higher temperatures in a shorter time under higher heating rates, and consequently the transient reaction rate increased with the increasing of heating rate. However, the pyrolysis of volatile and combustion of residual char was delayed due to the insufficient transfer of heat under high heat rates.

The maximum values of the second peak on GK, AS, and WP reaction curves were observed to be lower than other biomass, which was considered to be related to the lower fixed carbon content in these samples and namely less residual char was produced after pyrolysis. The reaction curve of CS was noted to be composed of three independent peaks. The former two peaks were considered as the pyrolysis of cellulose and hemicellulose, while the later peak was regarded as the combustion of char (Song and Hu 2003).

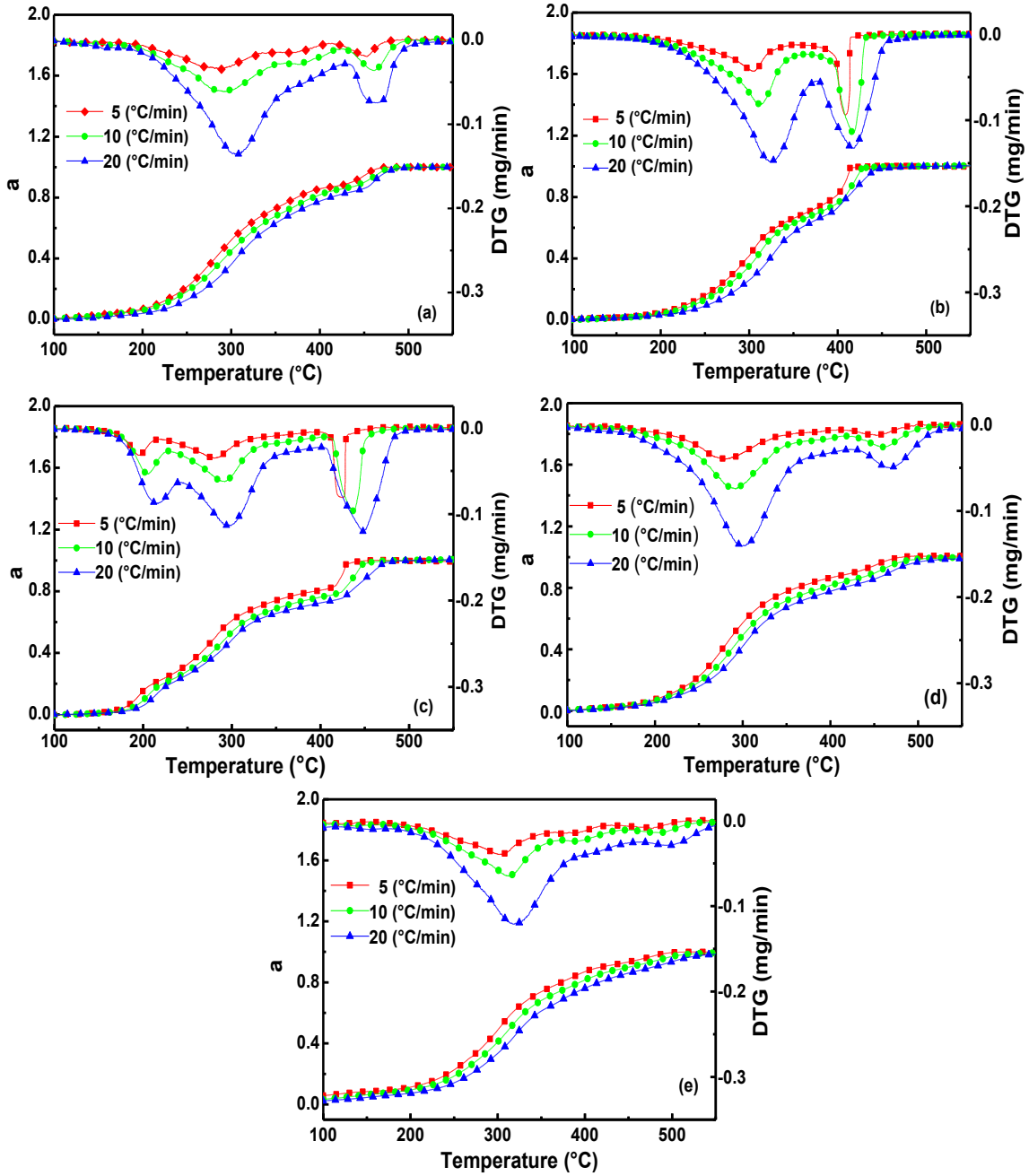

Fig. 2. Experimental fractional conversion and reaction rate curves of biomass: (a) GK; (b) PN; (c) CS; (d) AS; and (e) WP

The combustion characteristic parameters of biomass thermogravimetric experiments are exhibited in Table 2. It can be inferred that the initial and ultimate temperature as well as the maximum reaction rate temperature all increased with increasing of heating rate, which indicated that both the pyrolysis and combustion was lagged towards higher temperature zones. These changes was possibly owing to the inadequate transfer of heat in sample bed under high heating rate, while lower heat rate allows samples to have relatively longer time to react during heating process and namely a better thermal homogeneity during reaction (Hu *et al*. 2008).

Table 2. Thermogravimetric Combustion Parameters of Biomass Samples

Sample	Heating Rate (°C·min^{-1})	Volatile Combustion						Fixed Carbon Combustion				
		T_{1i} (°C)	T_{1max} (°C)	DTG_{1max} (mg/min)	T_{1e} (°C)	α_1	W_1 (mg)	T_{2max} (°C)	DTG_{2max} (mg/min)	T_{2e} (°C)	α_2	W_2 (mg)
GK	5	220.0	288.9	0.0348	407.8	0.865	4.33	447.6	0.0189	464.6	0.135	0.67
	10	226.4	289.6	0.0607	425.0	0.856	4.28	458.1	0.0356	478.2	0.144	0.72
	20	248.8	305.0	0.1361	436.4	0.840	4.20	463.8	0.0749	479.6	0.160	0.80
PN	5	184.1	307.1	0.0423	348.6	0.652	3.26	409.0	0.0943	416.0	0.348	1.74
	10	218.6	309.2	0.0808	359.8	0.647	3.24	417.5	0.1143	438.0	0.353	1.76
	20	246.0	323.2	0.1487	373.8	0.643	3.22	417.5	0.1319	461.1	0.357	1.88
CS	5	238.9	280.0	0.0389	387.9	0.788	3.94	423.8	0.0799	432.7	0.212	1.06
	10	265.7	292.1	0.0632	397.8	0.760	3.80	437.1	0.0968	450.7	0.240	1.20
	20	291.0	298.4	0.1196	401.3	0.728	3.64	448.3	0.1202	473.8	0.272	1.36
AS	5	221.4	280.4	0.0406	397.0	0.859	4.30	456.0	0.0129	478.8	0.141	0.70
	10	230.2	288.9	0.0741	415.3	0.840	4.20	457.4	0.0264	492.7	0.160	0.80
	20	238.8	302.2	0.1402	423.8	0.812	4.06	468.0	0.0482	507.7	0.188	0.94
WP	5	206.6	304.3	0.0397	430.0	0.914	4.57	476.5	0.0091	498.9	0.086	0.43
	10	216.9	316.2	0.0632	442.0	0.887	4.44	484.6	0.0140	524.7	0.113	0.66
	20	232.2	320.9	0.1193	454.6	0.870	4.35	494.5	0.0285	537.3	0.130	0.65

Notes: T_{1i} represents the ignition temperature; T_{1max} and T_{2max} represent the corresponding temperature of the first and second peak on reaction rate curve, respectively; DTG_{1max} and DTG_{2max} represent the reaction rates of the first peak and the second peak in the reaction rate curve, respectively; T_{1e} represents the temperature at which the first stage was completed; T_{2e} represents the burnout temperature; α_1 and α_2 represent the first and second stage conversion rate, $\alpha_2 = 1 - \alpha_1$; W_1 and W_2 represent the first and second stage mass loss.

Besides, the decomposition of GK, AS, and WP samples led to a conversion rate between 0.8 and 0.9, while that of PN and CS samples were 0.65 and 0.76 respectively. Above data revealed that about 90% weight loss of GK, AS, and WP took place in the form of volatile emission, and more char was generated from PN and CS after pyrolysis. Furthermore, the initial and ultimate combustion temperatures of chars from GK, AS, and WP biomass were relatively higher comparing to that from PN and CS samples, which manifested that the combustion of residue from PN and CS samples occurred more fiercely and namely a superior reactivity of chars from these two biomasses. The reaction of PN sample initiated and also completed at lower temperatures in comparison to other biomass samples, which demonstrated its superior reactivity during oxidative combustion.

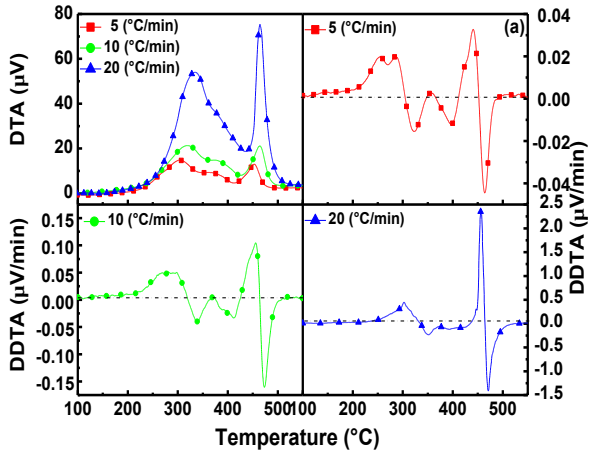

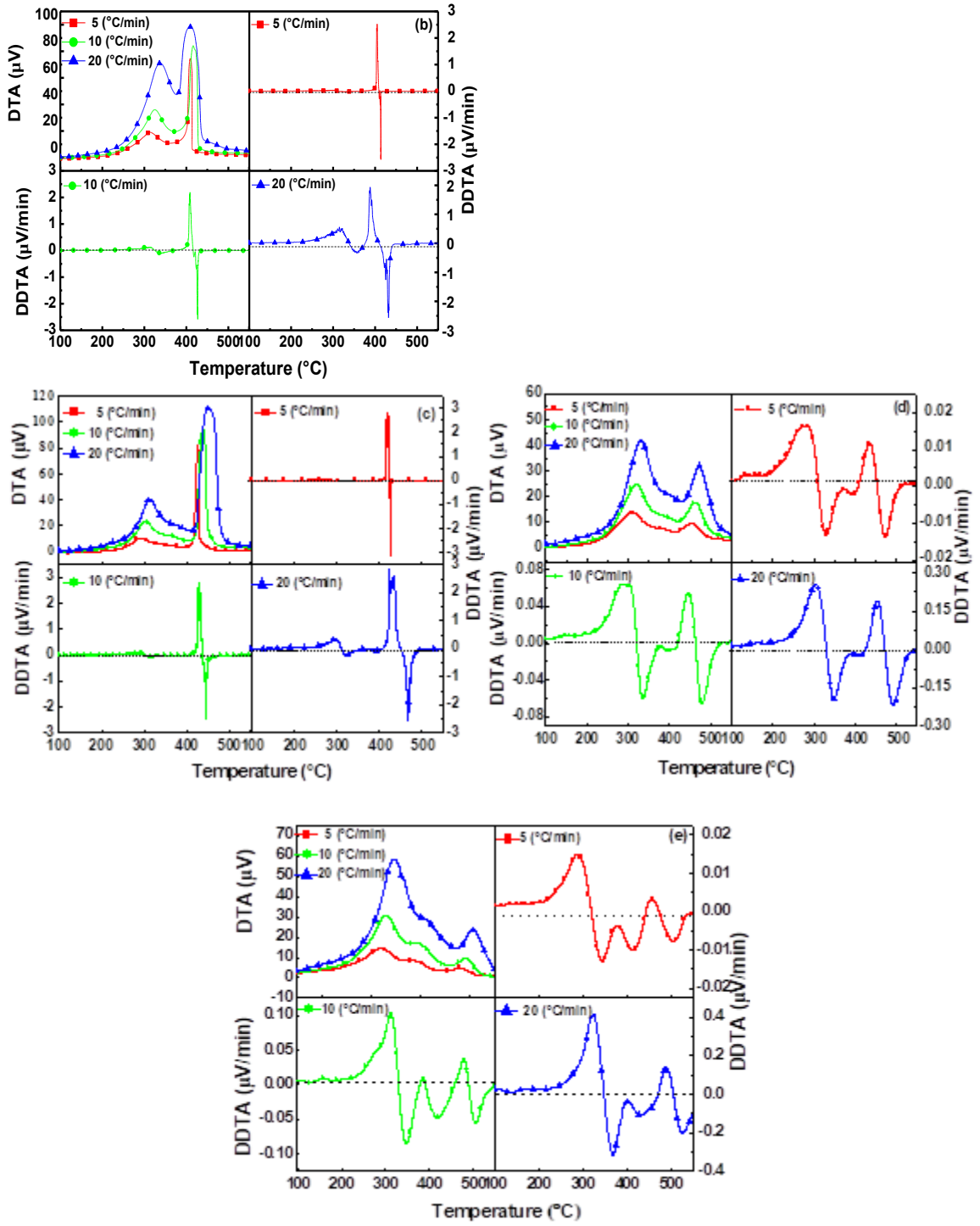

Fig. 3. The biomass the heat release curve of the sample: (a) GK; (b) PN; (c) CS; (d) AS; and (e) WP

Meanwhile, the temperature range in which the decomposition of PN and CS proceeded was significantly shortened with the increase of heating rate. Consequently, the restrictive link in decomposition process of PN and CS can be deduced as the transfer of heat. Similarly, the decomposition of other three biomasses and combustion of their chars were not significantly influenced by the variation of heating rate, which means that the combustion of these biomasses can only be facilitated by the optimization of kinetic

conditions. According to the data in Table 2, although the decomposition of WP started at a relatively lower temperature and achieved a maximum reaction rate over 0.12 mg/min, its ultimate combustion temperature was the highest of all. The phenomenon just described was observed from the char combustion peak on the reaction rate curve of WP, which indicated the inferior reactivity of char derived from WP.

Differential Thermal Analysis

Differential thermal analysis (DTA) was adopted to quantitatively compare the heat absorption and release behavior during the combustion of different biomass samples. The DTA curves and the differential of DTA (DDTA) of selected biomass samples are shown in Fig. 3. Though the difference in initial reaction temperature of biomass samples was significant, the maximum exothermic rate temperatures of selected samples were mainly concentrated at the ranges from 320 to 350 °C and 400 to 500°C due to the stage combustion of sample. It also is apparent that the corresponding temperatures of maximum exothermic rate temperatures also transferred towards high temperature zones with the increasing of heating rate, which was probably due to the delay combustion of sample under higher heating rates. The exothermic rate of WP, PN, and CS at the second weight loss stage was a direct reflection of the high combustion efficiency of char and also closely related to the burnout temperature of biomass samples. Meanwhile, the combustion sequence of components in samples was determined by comparing the variation on DDTA curves. As exhibited in Fig. 3, the DDTA curves of GK, AS, and WP consisted of three peaks, while just two independent peaks was observed on DDTA curves of PN and CS. The first peak around 300 °C was supposed to be categorized as the exothermic oxidation of hemicellulose, while the following two peaks at the temperatures of 400 °C and 450 °C were identified as the combustion of cellulose and lignin (Wang *et al*. 2014). With the increasing of heating rate, the combustion of hemicellulose in GK, AS, and WP samples occurred at a higher temperature and the exothermic rate became higher but the combustion of hemicellulose in the following stage was dramatically retarded with the increasing of heating rate. This phenomenon was possibly related to the temperature gradient produced by the inadequate transfer of heat, which postponed the reaction of cellulose as well as lignin into high temperature zones. Consequently, the release of heat over 450 °C was remarkably increased. Nevertheless, due to the advantage in reactivity of functional groups, an opposite trend was observed during the combustion of PN and CS. The combustion of hemicellulose was intensified with the increasing of heating rate, while the reaction rate of cellulose was reduced by the intermittent of heat.

Kinetic Analysis

In order to clarify the non-isothermal combustion mechanism of biomass samples, the FWO reaction model was introduced for the kinetic calculations in this research. As known, the relationship among reaction rate, reaction rate constant and conversion rate can be described as a linear function, which is shown in Eq. 2.

$$\frac{d\alpha}{dt} = k(T)f(\alpha) \quad (2)$$

where α represents the conversion rate of sample during combustion, t represents the heating time required for conversion rate to reach α, T represents the temperature at which conversion rate reaches α, and $f(\alpha)$ represents the reaction mechanism function.

The rate constant k(T) is typically expressed according to the Arrhenius formula

as shown in Eq. 3.

$$k(T) = A \exp(-\frac{E}{RT}) \quad (3)$$

where A represents the pre-exponential factor, E represents the activation energy, and R represents the gas reaction constant, which is 8.314×10^{-3}kJ/(mol·K).

The kinetic equation expressed in Eq. 4 can be derived by substituting Eq. 3 into Eq. 2.

$$\frac{d\alpha}{dt} = A \exp\left(-\frac{E}{RT}\right) f(a) \quad (4)$$

The heating rate of a non-isothemal reaction can be calculated by Eq. 5.

$$\beta = \frac{dT}{dt} \quad (5)$$

A non-isothermal kinetic equation as Eq. 6 can be obtained by substituting Eq. 5 into Eq. 4.

$$\frac{d\alpha}{dT} = \frac{A}{\beta} \exp\left(-\frac{E}{RT}\right) f(a) \quad (6)$$

The activation energy of a non-isothermal thermogravimetric reaction can be calculated with FWO equation based on equal conversion rate method, which is described Eq. 7.

$$\ln \beta = \ln \frac{0.0048AE}{RG(\alpha)} - 1.0516 \frac{E}{RT} \quad (7)$$

For a certain α, the linear relationship between lnβ and 1/T can determined by fitting the data under several heating rates, while the value of activation energy can be calculated by the slope of the fitting plots. The experimental data and fitting plots are exhibited in Fig. 4.

It should be noted that the variation in activation energy of all biomass samples showed a multiple-parabola law with the increasing of conversion rate, while an evident consistency between the corresponding temperature of maximum activation energy and maximum reaction rate was also observed in the comparison between the data in Table 3 and Fig. 2. This phenomenon was possibly due to the exhaust of activated molecules in fuel and also the barricade on the surface layer created by mineral residue produced by the consumption of combustible matters. Consequently, the reaction rate of sample dramatically decreased with the further increasing of conversion rate. As a result, the activation energy of sample for succeeding reactions increased with the extending of combustion after the maximum reaction rate. All combustion reactions of biomass samples consisted of at least two stages of weight loss, which was responsible for the repetitive variation of activation energy.

Meanwhile, though the combustion of PN and CS sample completed at a early stage of heating, their average activation energy was relatively higher comparing to some biomasses. It is considered that the combustion reaction of PN and CS occurred in a lower temperature range, in which the average energy of molecule in biomass samples was lower for the insufficient thermal motion of molecules. Therefore, more energy is required to activate the molecules of sample for combustion in low temperature environment.

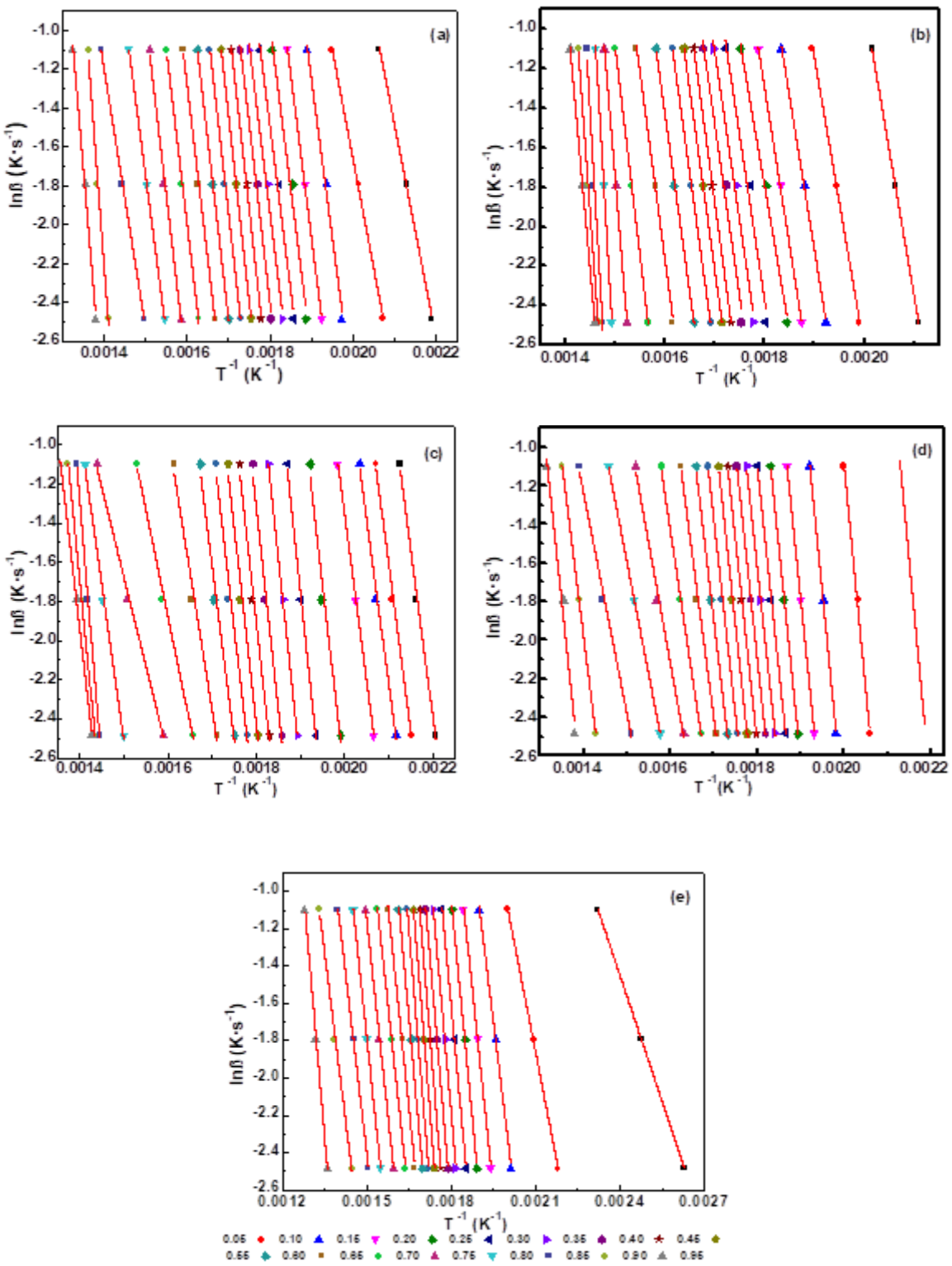

Fig. 4. Fitting relationship between lnβ and 1/T: (a) GK; (b) PN; (c) CS; (d) AS; and (e) WP

Table 3. Activation Energy and Correlation Coefficient of Biomass Under Corresponding Rate

α	GK		PN		CS		AS		WP	
	E (kJ/mol)	R^2	*E* (kJ/mol)	R^2	*E* (kJ/mol)	R^2	*E* (kJ/mol)	R^2	*E* (kJ/mol)	R^2
0.05	86.53	0.9965	116.91	0.9999	134.93	0.9874	189.01	0.9815	35.62	0.9999
0.10	88.98	0.9976	116.25	0.9964	134.76	0.9934	184.07	0.9926	61.13	0.9994
0.15	127.93	0.9927	122.89	0.9983	132.92	0.9920	181.06	0.9999	96.59	0.9953
0.20	132.87	0.9972	126.03	0.9994	134.45	0.9998	174.05	0.9997	113.39	0.9962
0.25	132.49	0.9675	116.41	0.9922	154.66	0.9608	174.09	0.9980	123.55	0.9949
0.30	133.99	0.9814	131.84	0.9647	166.26	0.9920	168.15	0.9984	128.57	0.9985
0.35	136.38	0.9815	135.84	0.9709	168.50	1.0000	165.34	0.9950	135.38	0.9964
0.40	145.89	0.9900	137.91	0.9672	162.27	0.9627	167.02	0.9982	139.46	0.9990
0.45	152.15	0.9974	146.49	0.9995	159.90	0.9714	166.04	0.9951	145.81	1.0000
0.50	151.79	1.0000	143.33	1.0000	158.86	0.9722	166.42	0.9911	147.29	1.0000
0.55	148.83	0.9993	143.70	0.9995	153.51	0.9631	160.83	0.9928	144.36	0.9999
0.60	145.94	0.9986	143.71	0.9967	139.69	0.9619	151.12	0.9914	131.56	0.9966
0.65	142.29	0.9966	149.33	0.9943	111.20	0.9746	134.76	0.9928	114.89	0.9906
0.70	141.48	0.9895	167.62	0.9985	86.13	0.9913	118.55	0.9946	109.65	0.9968
0.75	143.51	0.9929	242.56	0.9975	72.16	0.9913	98.72	0.9891	109.72	0.9994
0.80	128.08	1.0000	337.62	0.9977	125.75	0.9915	91.95	1.0000	112.55	1.0000
0.85	105.33	0.9998	338.08	0.9725	215.18	0.9975	90.61	0.9925	101.17	0.9992
0.90	223.85	0.9740	275.30	0.9959	181.60	1.0000	141.77	1.0000	95.26	0.9909
0.95	199.31	0.9892	220.94	0.9991	153.20	0.9966	168.04	0.9680	138.19	0.9974
Aver-age	140.40	0.9917	174.36	0.9916	144.52	0.9842	152.19	0.9932	114.95	0.9974

Functional Group Structure Analysis

The functional group structure of the biomass samples was detected by Fourier-transform infrared spectroscopy (FTIR) carried out on a Cary 630 FTIR (Agilent Technologies Inc, Shanghai, China) in the spectral wavelength range of 400 to 4000 cm^{-1}. To ensure an ideal reproducibility of experimental results, each test was repeated at least three times before a final result was ascertained. The FTIR results of the biomass samples are shown in Fig. 5, while the characteristic peak values and corresponding functional groups are listed in Table 4 (Yu 2006).

It can be seen from the FTIR spectra that the peak intensity of aromatic hydrocarbon around 1590 cm^{-1} on spectra of PN and CS samples was relatively lower than that of other biomass samples, which indicated that the numbers of benzene rings in PN and CS samples were inferior. For the decomposition of aromatic hydrocarbon usually occurs in under high temperatures due to the high stability of conjugated π bond and hexatomic ring and consequently the reactivity of fuels with high content of aromatic hydrocarbon is supposed to be lower. Furthermore, -OH is a radical with high reactivity for the breakage of H-O bond take places at a temperature as low as 200 °C (Min and Zhang 2005) and the -OH absorbance of PN and CS samples around 3400 cm^{-1} was also noticed to be strong. Namely, the functional groups in PN and CS samples can be considered as mainly high reactivity radicals, which explained not only the high reaction rate of PN and CS samples in the temperature range between 200 and 300 °C but also the lower burnout temperature of these two biomasses. However, the absorbance of the peaks

around 1040cm^{-1} on spectra of GK, PN and CS samples was observed to be strong, namely the mineral ash content in these three biomass was higher than that of AS and WP. The findings described above show a great accordance with the proximate analysis and the reaction temperature analysis results of selected samples in Tables 1 and 2. In addition, the heat released during combustion is closely related to the formation of functional groups for the generation of heat during the breakage of different chemical bonds varies dramatically. Therefore, although the carbon content of PN and CS samples were higher, the carbon atoms in these samples mainly existed in the form of low calorie radicals like -OH and -CH_3. It is possibly the reason for the low HHV of PN and CS during oxidation combustion.

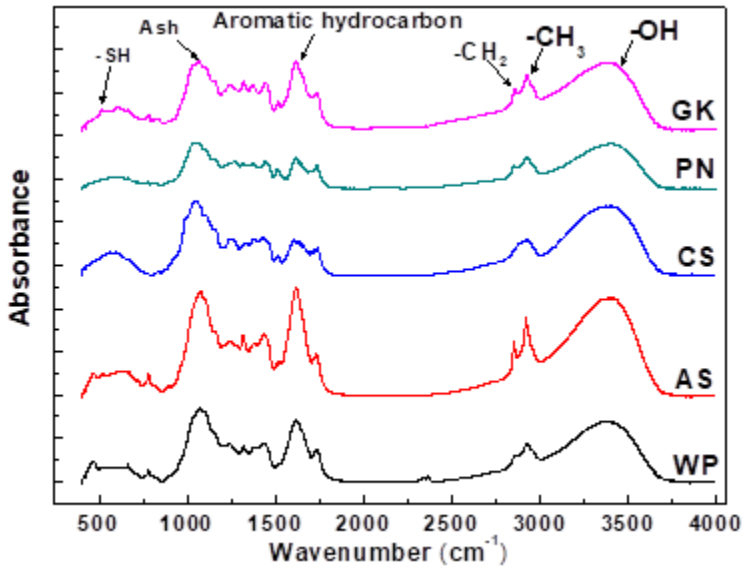

Fig. 5. FTIR spectra of biomass samples

Table 4. Classification of Absorption Peak in FTIR Spectra

Peaks	Wavenumber (cm^{-1})	Functional Groups
1	3550-3200	-OH
	3030	-CH (aromatic ring)
2	2950(shoulders)	-CH_3
3	2920,2860	-CH_3 Cycloalkanes or aliphatic hydrocarbons
4	2858-2847	-CH_2
5	2780-2350	-COOH
6	1610	Carbonyl substituted aromatic hydrocarbons
	1590-1470	Aromatic hydrocarbon
	1460	-CH_2,-CH_3, Inorganic carbonate
7	1375	-CH_3
8	1330-1110	C-O (Phenols, alcohol ethers, lipids)
	1040-900	Ash
9	860	CH (1,2,4-;2,4,5;1,2,3,4,5 substituted aromatic hydrocarbons)
	750	CH (1,2 Substituted aromatic hydrocarbons)
	700	CH (Single substituted or 1,3 substituted aromatic hydrocarbons)
10	475	-SH

For a more detailed understanding of the specific distribution of the functional groups in the material, all spectra were divided into four regions: aromatic structures (700 to 900 cm^{-1}), oxygen-containing structures (1000 to 1800 cm^{-1}), aliphatic structures (2800 to 3000 cm^{-1}), and hydroxyl structures (3000 to 3600 cm^{-1}). PeakFit software (Second edition, SeaSolve Software Inc, Framingham, MA, America) was applied for the deconvolution process of all spectra and also the area calculations of derived peaks. The deconvolution process of WP sample is shown in Fig. 6 as an example, while the correlation coefficients between the experimental and fitting curves all exceeded 0.98. Equations from 8 to 14 were used to calculate the functional groups structural parameters of the biomass samples (He *et al*. 2017), while the calculation results are exhibited in Table 5.

The apparent aromaticity f_a was used to characterize the aromatic carbon fraction to determine the aromatic structure parameters. According to Wang *et al*. (2011), all carbon atoms are considered as aromatic (C_{ar}) carbon or aliphatic (C_{al}) carbon and f_a can be calculated using Eqs. 8 through 10,

$$\frac{H_{al}}{H} = \frac{H_{al}}{H_{al}+H_{ar}} = \frac{A_{2800-3000}}{A_{2800-3000}+A_{700-900}} \quad (8)$$

$$\frac{C_{al}}{C} = \left(\frac{H_{al}}{H} \times \frac{H}{C}\right) / \left(\frac{H_{al}}{C_{al}}\right) \quad (9)$$

$$f_a = 1 - \frac{C_{al}}{C} \quad (10)$$

where H_{al}/H represents the ratio between aliphatic (H_{al}) and total hydrogen atoms (H). The distribution aliphatic hydrogen (H_{al}) concentrates in the wavenumber range between 2800 and 3000 cm^{-1}, while the fluctuation between wavenumber of 700 and 900 cm^{-1} belongs to absorbance of aromatic hydrogen (H_{ar}), C_{al}/C represents the ratio between aliphatic and total carbon, H/C represents the ratio between hydrogen and carbon atoms determined from the ultimate analysis, H_{al}/C_{al}, with a fixed value of 1.8, represents the ratio between hydrogen and carbon in aliphatic groups, $A_{3000\text{-}2800}$ represents the integrated area between 3000 and 2800 cm^{-1}, which is used to estimate the total aliphatic content (CH_3, CH_2, and CH).

The aromatic C=C band intensity is related to the area under the peaks located at 1600 cm^{-1} (A_{1600}) and the degree of condensation (DOC) of the aromatic rings can be determined through Eq. 11:

$$DOC = \frac{A_{700-900}}{A_{1600}} \quad (11)$$

According to the ratio between CH_2 and CH_3, namely the area ratio of $A(CH_2)/A(CH_3)$, the aliphatic group length and the branched chain degree were calculated to determine the aliphatic structural parameters. A greater ratio of $A(CH_2)/A(CH_3)$ indicates a longer aliphatic chain of the aromatic ring. In contrast, a smaller space between the aromatic rings and the relatively dense structure were indicated. The intensity ratio of CH_2 / CH_3 was determined by Eq. 12,

$$\frac{A(CH_2)}{A(CH_3)} = \frac{A_{2915-2940}}{A_{2950-2975}} \quad (12)$$

where $A_{2915\text{-}2940}$ and $A_{2950\text{-}2975}$ are attributed to the asymmetric stretching intensity of CH_2 and CH_3 groups, respectively.

The structural parameter '*C*' of the oxygen-containing functional group

represented the change in the ratio from the C=C to the C=O group to determine the structural parameters of the oxygen-containing functional and calculated through Eq. 13,

$$'C' = \frac{A_{1650-1800}}{A_{1650-1800} + A_{1600}} \quad (13)$$

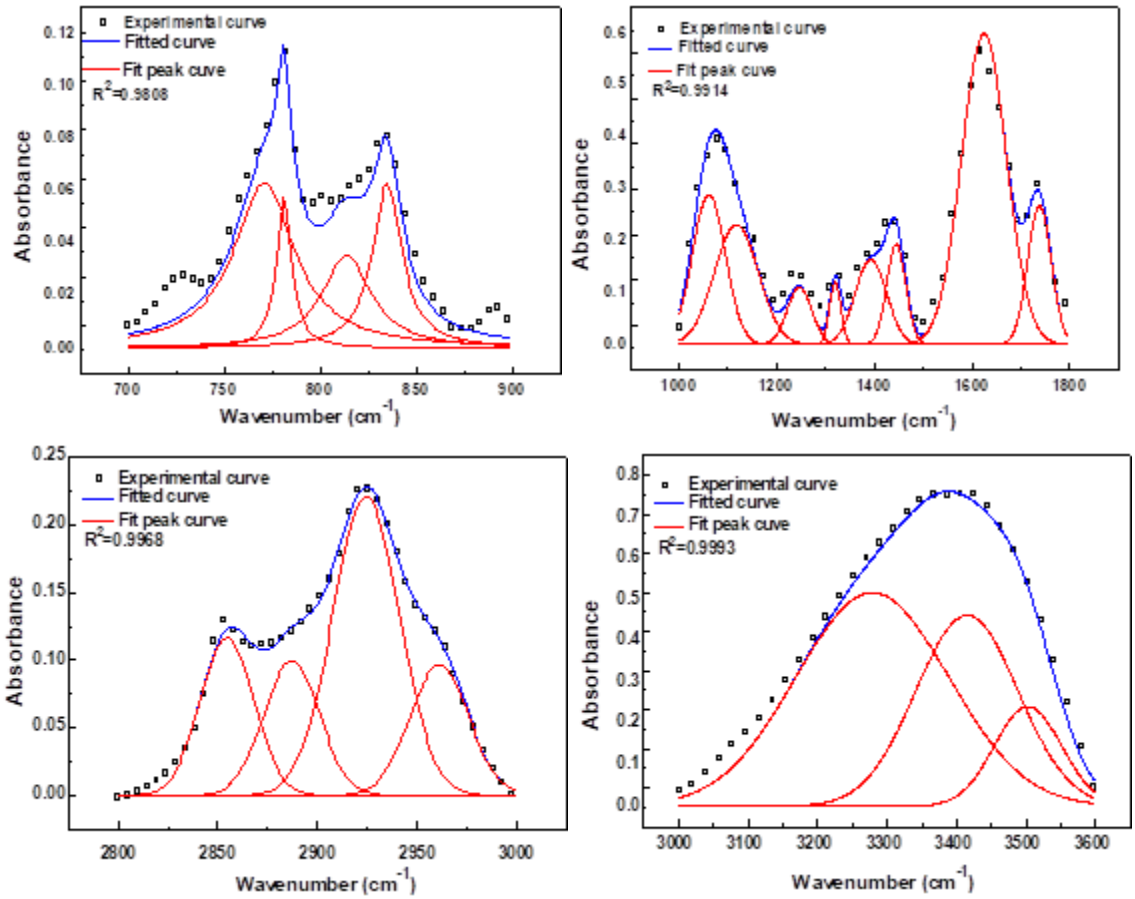

Fig. 6. Deconvolution process on FTIR spectrum of WP

Table 5. Structure Parameters of Biomass Infrared Spectra

Sample	f_a	*DOC*	$A(CH_2)/A(CH_3)$	*'C'*
GK	0.941	0.107	2.748	0.416
PN	0.874	0.103	1.605	0.579
CS	0.932	0.079	1.522	0.586
AS	0.849	0.078	3.225	0.535
WP	0.895	0.105	2.604	0.553

As shown in Table 5, the f_a value of CS was higher than that of PN, which indicated that higher proportion of carbon atoms in CS mainly existed in the form of aromatic hydrocarbon comparing to that of PN. Namely, the radicals in CS required higher temperatures to complete combustion and hence the burnout temperature of PN was 17 °C lower than that of CS. The relationship between area ratio of aromatic C-H and aromatic C=C showed that DOC of CS and AS was lower than other biomass samples, which meant that the reactivity of aromatic groups in CS and AS samples were supposed to be higher during reaction and accordingly the reaction rate of char from CS

was also observed to be faster during combustion. However, the combustion rate of char from AS was not that significant for the low proportion of aromatic groups in AS. Besides, the value of $A(CH_2)/A(CH_3)$ was calculated by the area ratio of peaks located at 2915-2940 and 2950-2975 cm^{-1}, which is considered to be related to the length of aliphatic chains or the degree of branching aliphatic side-chains (José *et al*. 1994). The higher $A(CH_2)/A(CH_3)$ values of GK, AS and WP implied that the content of methyl groups in these biomasses was much lower than that of PN and CS for carbon atoms in GK, AS and WP are mainly in the form of aromatic hydrocarbon. Meanwhile, the difference in value of 'C' showed that the number of oxygen-containing functional groups in PN and CS was lower in comparison to other three biomasses and was responsible for the lower HHV of PN and CS, which exhibited a good accordance with the ultimate analysis results in Fig. 1 (Chen *et al*. 2012). The value of 'C' of GK was the lowest though its oxygen content was the highest in all five biomass samples. This was probably because that the oxygen in GK was mainly in the form of -OH and therefore a high conversion rate was achieved at the temperature around 400 °C.

CONCLUSIONS

1. The combustion of PN and CS was completed at a lower temperature range compared to the ultimate combustion temperature of GK, AS, and WP due to their advantage of high reactivity radicals in functional group structure. Simultaneously, the differences in chemical combinations of C, H, and O atoms in fuel also has a dominant effect on the exothermic behavior of biomass during combustion. Hence, more heat can be obtained during the combustion of AS and WP due to their high content of aromatic hydrocarbon in function groups.
2. Due to the difference in functional groups structures, variation of heating rate produced an opposite effect for different biomass samples. The combustion of volatile and char in GK, AS, and WP transferred to high temperature zones with the increasing of heating rate. Consequently, the exothermic rate in high temperature range between 450 and 500 °C was significantly intensified. However, the increasing of heating rate isolated the combustion of volatile and char in PN and CS, which increased the exothermic rate of volatile around 300 °C but decreased exothermic rate of char in high temperature zones above 400 °C
3. The combustion of PN, CS and AS samples is stable under different heating rates for their functional groups are mainly composed of high reactivity radicals, namely a superior combustion rate of these biomasses can be achieved at a low heating rate. Both of the initial and ultimate combustion temperatures of GK and WP were significantly increased with the increasing of heating rate, which indicated that higher reaction temperature is required if GK and WP are utilized as fuel in civil or industrial scales.

ACKNOWLEDGMENTS

The authors thank team partners from the Research Institute of Mass Energy Optimization and New Technology of Metallurgy for their valuable contribution to this work and preparation of this paper. This work was financially supported by National Natural Science Foundation of China (51874171, 51504132, 51674139, 51604148) and supported by the University of Science and Technology Liaoning Talents program.

REFERENCES CITED

Abbasi, T., and Abbasi, S. A. (2010). "Biomass energy and the environmental impacts associated with its production and utilization," *Renewable and Sustainable Energy Reviews* 14(3), 919-937. DOI: 10.1016/j.rser.2009.11.006

Caputo, A. C., Palumbo, M., Pelagagge, P. M., and Scacchia, F. (2005). "Economics of biomass energy utilization in combustion and gasification plants: Effects of logistic variables," *Biomass and Bioenergy* 28(1), 35-51. DOI: 10.1016/j.biombioe.2004.04.009.

Chen, Y., Mastalerz. M., and Schimmelmann, A. (2012). "Characterization of chemical functional groups in macerals across different coal ranks via micro-FTIR spectroscopy," *International Journal of Coal Geology* 104(none). DOI: 10.1016/j.coal.2012.09.001.

Emre, Ö., Sharon, F. M., Bruceg. M., and Mustafa. V. K. (2012). "Thermal analysis of co-firing of oil shale and biomass fuels," *Oil Shale* 29(2), 190-201. DOI: 10.3176/oil.2012.2.07.

Hoel, M. (1996). "Depletion of fossil fuels and the impacts of global warming," *Resource and Energy Economics* 18(2), 115-136. DOI: 10.1016/0928-7655(96)00005-X

Hu, R. Z., Gao, S. L., and Zhao, F. Q. (2008). Thermal analysis kinetics, (Second edition). Science press, (http://bookask.com/book/1674416.html).

He, X. Q., Liu, X. F., Nie, B. S., and S, D. Z. (2017). "FTIR and Raman spectroscopy characterization of functional groups in various rank coals," *Fuel* 206(10), 555-563. DOI:10.1016/j.fuel.2017.05.101

José, V, I., Moliner, R., and Bonet, A. J. (1994). "FT-IR investigation on char formation during the early stages of coal pyrolysis," *Fuel* 73(6), 918-924. DOI: 10.1016/0016-2361(94)90287-9.

Kandasamy, J., Mustafa .V. K., and Iskender. G., (2017). "Combustion properties and kinetics of different biomass samples using TG–MS technique," *Journal of Thermal Analysis and Calorimetry* 127(2), 1361–1370. DOI 10.1007/s10973-016-6042-1.

Liu, Z. X., Niu, W. J., Chu, H. Y., and Niu, Z. Y. (2018) "Optimization of straw pyrolysis process and analysis of physicochemical properties of biochar," *Journal of Agricultural Engineering* 34(5), 196-203. DOI: 10.11975/j.issn.1002-6819.2018.05.026

Min, F. F., and Zhang, M. X. (2005). "Study on biomass combustion mode and combustion characteristics," *Journal of Coal* 30(1), 104-108. DOI: 10.3321/j.issn:0253-9993.2005.01.023

Mustafa, V. K., and Emre, O. (2017). "Characterization of lignocellulose biomass and model compounds by thermogravimetry," *Energy Sources* 39(2), 134-139. DOI: 10.1080/15567036.2016.1214643.

Mustafa, V. K., and Emre, O. (2013). "Thermal analysis and kinetics of biomass samples," *Fuel Processing Technology* 106(2), 739-743. DOI: 10.1016/j.fuproc.2012.10.010

Qin, L., Zhang, S., Gao, Z., and Jiang, E. (2017). "Molding fuel and combustion characteristics of biochar and lignin," *Transactions of the Chinese Society for Agricultural Machinery* 48(4), 276-283. DOI: 10.6041/j.issn.1000-1298.2017.04.036

Song, C. C., and Hu, H, Q. (2003). "Studies on catalytic pyrolysis and kinetics of straw and its main components," *Coal Conversion* 26(3), 91-97. DOI: 10.3969/j.issn. 1004-4248.2003.03.020

Wang, R., Tian, Y. S., Zhao, L. X., Yao, Z. L., Meng, H. B. and Hou, S. L. (2014). "Biomass industrial analysis and calorific value measurement based on thermogravimetric method," *Journal of Agricultural Engineering* 30(5), 169-177. DOI: 10.3969/j.issn.1002-6819.2014.05.022

Wang, S. Q., Tang, Y. G., Schobert, H. H., Guo, Y. N. (2011). "FTIR and ^{13}C NMR Investigation of coal component of late Permian coals from southern China," *Energy & Fuels* 25(12), 5672-5677. DOI: 10.1021/ef201196v.

Ying, H., and Jiang, J. C. (2007). "Biomass energy conversion technologies and applications (IV) - Biomass pyrolysis gasification technology research and application," *Biomass Chemical Engineering* 9(6), 47-55. DOI: 10.3969/j.issn.1673-5854.2007.06.012

Yu, J. S. (2006). *Coal Chemical Industry*, Metallurgical Industry Press, Beijing.

Zhou, Z. R., and Wu, W. L. (2005). "Status quo and prospects of biomass energy," *Transactions of the Chinese Society of Agricultural Engineering* 21(12), 12-15. DOI: 10.1007/s10971-005-6694-y

Zeng, X., Ma, Y., and Ma, L. (2007). "Utilization of straw in biomass energy in China," *Renewable & Sustainable Energy Reviews* 11(5), 976-987. DOI: 10.1016/j.rser.2005.10.003

Zhang, Y. L., Huang, R. J., El Haddad, I., Ho, K. F., Cao, J. J., Han, Y., Zotter, P., Bozzetti, C., Daellenbanch, R. K., Canonaco, F., *et al*. (2015). "Fossil *vs*. non-fossil sources of fine carbonaceous aerosols in four Chinese cities during the extreme winter haze episode of 2013," *Atmospheric Chemistry and Physics* 15(3), 1299-1312. DOI: 10.5194/acp-15-1299-2015

Article submitted: April 5, 2019; Peer review completed: June 16, 2019; Revised version received and accepted: July 30, 2019; Published: August 7, 2019.
DOI: 10.15376/biores.14.4.7702-7718